

# Fox–Wolfram Moments in Higgs Physics

Catherine Bernaciak,<sup>1</sup> Malte Seán Andreas Buschmann,<sup>1</sup> Anja Butter,<sup>1</sup> and Tilman Plehn<sup>1</sup>

<sup>1</sup>*Institut für Theoretische Physik, Universität Heidelberg, Germany*

Geometric correlations between jets as part of hard processes or in addition to hard processes are key ingredients to many LHC analyses. Fox–Wolfram moments systematically describe these correlations in terms of spherical harmonics. These moments, either computed from the tagging jets or from all jets in each event, can significantly improve Higgs searches in weak boson fusion. Applications of Fox–Wolfram moments in LHC analyses obviously surpass jets as analysis objects as well as Higgs searches in terms of analyses.

## Contents

<b>I. Introduction</b>	2
<b>II. Fox–Wolfram moments</b>	2
<b>III. Two tagging jets</b>	6
<b>IV. All jets</b>	9
<b>V. Outlook</b>	11
<b>Acknowledgments</b>	12
<b>References</b>	12

## I. INTRODUCTION

Fox–Wolfram moments are an established tool to analyze geometric patterns in QCD [1], but have never been employed at the LHC [2]. The structure of jet activity in association with a hard process is a crucial feature for many LHC analyses, in the Higgs sector [3, 4] as well as in new physics searches [5]. For example, the Higgs discovery by ATLAS [6] and CMS [7] relied on information about jets produced in association with the Higgs boson in several different channels. The most established LHC search based on information from additional jets is weak-boson-fusion (WBF) Higgs production [8–10], *i.e.* Higgs production together with two relatively hard forward tagging jets [11]. In addition to the two forward tagging jets WBF Higgs production predicts a lack of central jet activity between them [12–14]. We propose to analyze the jet activity for example in WBF Higgs production based on the general framework of Fox–Wolfram moments [1, 2]. For our first study of the jet geometry this process has the advantage that it includes jets with very different origin: the WBF Higgs signal uses two tagging jets from the hard process, its  $Z$ +jets background comes with two radiated QCD jets, and in the  $t\bar{t}$  background at least one decay jet acts as a tagging jet.

Fox–Wolfram moments originate in an expansion of jet–jet correlations in terms of spherical harmonics. They are constructed by summing all jet–jet correlations over all  $2\ell + 1$  directions with a momentum dependent weight. This way they are sensitive to the number of jets in the final state, their angular correlation, and their energy distribution. Historically, Fox–Wolfram moments have been an alternative to the usual event shapes [15]. They were tested in the ALEPH Higgs search in the four-jet channel, but did not get used in the final analysis. On the other hand, with some definition of the weight they are available in PYTHIA [16] and have been used in  $B$  physics. The question is what we can learn from them for Higgs physics at the LHC.

The objects which enter the computation of Fox–Wolfram moments do not have to be jets. Because they are closely related to event shapes it is even likely that some kind of calorimeter entry, particle flow object, or topocluster will eventually turn out to be more efficient. We make our first case based on jets because jets allow us to relatively easily reduce effects from underlying event and pile-up on the moments. Keeping all jets hard and well separated also ensures that perturbative QCD is applicable, so we can trust the predictions from standard QCD Monte Carlo generators with a parton shower.

The structure of this paper is simple. First, we introduce the Fox–Wolfram moments and determine what kind of weight factors are most appropriate for our purpose. Then we compute Fox–Wolfram moments from the two tagging jets alone and test how they can improve the WBF Higgs analysis. Finally, we repeat this analysis with moments including correlations between all observed jets.

## II. FOX–WOLFRAM MOMENTS

For many decades we have known that QCD events can be very efficiently described by the geometry of the partons. This geometry can be analyzed at the level of energy deposition, using event shapes, or based on reconstructed jets. At the LHC the latter have the advantage that effects from underlying event and pile-up should be easier to remove. Therefore, we will in this paper focus on the geometric correlations between jets.

For example, cosmological analyses parameterize angular correlations in terms of spherical harmonics. Fox–Wolfram moments are based on a superposition of spherical harmonics,  $Y_\ell^m(\theta, \phi)$ , where  $\theta$  and  $\phi$  are the usual spherical coordinates. They were originally defined as [1]

$$H_\ell = \frac{4\pi}{2\ell + 1} \sum_{m=-\ell}^{\ell} \left| \sum_{i=1}^N Y_\ell^m(\Omega_i) \frac{|\vec{p}_i|}{\sqrt{s}} \right|^2, \quad (1)$$

where the index  $i$  sums over all final state objects which can be defined anywhere at the detector or jet level. In Sec. III we will start by limiting ourselves to Fox–Wolfram moments computed from the two tagging jets ( $N = 2$ ) while in Sec. IV we will also include additional QCD jets with an event-by-event choice of  $N$ . The angular distance  $\Omega_i$  assumes a reference axis which as we will see drops out. The denominator  $\sqrt{s}$  is the energy of all states  $i$ , ensuring the normalization  $0 < H_\ell < 1$ . The weight factor  $|\vec{p}_i|/\sqrt{s}$  is only one possible choice so we will adapt it to hadron collider physics later.

We can rewrite Eq.(1) to express the dependence on the total angle between each final state object using the addition theorem for spherical harmonics

$$\begin{aligned} H_\ell &= \sum_{i,j=1}^N \frac{|\vec{p}_i| |\vec{p}_j|}{\sqrt{s} \sqrt{s}} \frac{4\pi}{2\ell+1} \sum_{m=-\ell}^{\ell} Y_\ell^m(\Omega_i) Y_\ell^{m*}(\Omega_j) \\ &= \sum_{i,j=1}^N \frac{|\vec{p}_i| |\vec{p}_j|}{s} P_\ell(\cos \Omega_{ij}) , \end{aligned} \quad (2)$$

with the distance measure  $\cos \Omega_{ij} = \cos \theta_i \cos \theta_j + \sin \theta_i \sin \theta_j \cos(\phi_i - \phi_j)$ .

At hadron colliders it may be better to use a weight based on the products of transverse momenta and normalized to their squared sum [2]. We study different weight factors  $W_{ij}$ , namely

$$H_\ell^x = \sum_{i,j=1}^N W_{ij}^x P_\ell(\cos \Omega_{ij}) , \quad (3)$$

with the specific choices

$$\begin{aligned} W_{ij}^s &= \frac{|\vec{p}_i| |\vec{p}_j|}{s} = \frac{|\vec{p}_i| |\vec{p}_j|}{(\sum p_i)^2} & W_{ij}^p &= \frac{|\vec{p}_i| |\vec{p}_j|}{|\vec{p}|_{\text{tot}}^2} = \frac{|\vec{p}_i| |\vec{p}_j|}{(\sum |\vec{p}_i|)^2} \\ W_{ij}^T &= \frac{p_{Ti} p_{Tj}}{p_{T,\text{tot}}^2} = \frac{p_{Ti} p_{Tj}}{(\sum p_{Ti})^2} & W_{ij}^z &= \frac{p_{zi} p_{zj}}{p_{z,\text{tot}}^2} = \frac{p_{zi} p_{zj}}{(\sum p_{zi})^2} \\ W_{ij}^y &= \frac{|y_i - \bar{y}|^{-1} |y_j - \bar{y}|^{-1}}{(\sum |y_i - \bar{y}|^{-1})^2} & W_{ij}^1 &= 1 \end{aligned} \quad (4)$$

For the rapidity-based weight we use  $\bar{y}$  for the average rapidity of the two tagging jets.

To compare the performance of the different weights listed in Eq.(4) we need a reference process at the LHC. Higgs searches use the QCD structure of signal events in the search for weak-boson-fusion Higgs production [8, 9, 17]. This is why we use it, with a decay  $H \rightarrow \tau^+ \tau^-$  as the reference channel for our feasibility study. The Higgs decay products do not enter our analysis; to define the backgrounds we assume that both of the taus decay leptonically. Two major background processes with distinctly different jet geometries are  $Z + n$  jets production at order  $\alpha\alpha_s^n$  and top pair production [9]. Again, we do not include the  $Z \rightarrow \tau^+ \tau^-$  decays or the  $W \rightarrow \tau \nu$  decays, but we do include the corresponding branching ratios for  $H, Z \rightarrow \tau^+ \tau^-$  and  $t\bar{t} \rightarrow b\bar{b}\ell^+\ell^-\bar{\nu}\nu$  in all total cross section results shown. Our focus is on the jets from the hard process of the Higgs signal, the QCD jet radiation in the  $Z$ +jet process and the decay jets in addition to the QCD jet radiation in top pair production. From jet scaling studies we know that the number of jets and their transverse momentum spectra are very different [12, 13]. Using the Fox–Wolfram moments we focus on their angular correlations.

We use SHERPA [18] with CKKW merging [19] to generate merged samples of WBF  $H$  plus up to three hard jets,  $Z$  plus up to two hard jets and  $t\bar{t}$  plus up to one hard jet. Subsequent parton showering and hadronization is modeled also with SHERPA. For jet clustering, we use an anti- $k_T$  algorithm as implemented in FASTJET [20] with  $R = 0.4$ , *i.e.* the size of the jets will be small compared to their separation.

Our signature consists of two (central) Higgs decay products plus two tagging jets. The acceptance cuts for the two tagging jets are

$$p_{Tj} > 20 \text{ GeV} \quad |y_j| < 5.0 \quad \Delta R_{j_1 j_2} > 0.7 . \quad (5)$$

In addition to these minimal cuts we account for the tagging jet geometry by placing an additional cut on their invariant mass,

$$m_{j_1 j_2} > 600 \text{ GeV} . \quad (6)$$

Usually, WBF analyses apply two additional conditions on the tagging jets, namely

$$\begin{aligned} y_{j_1} \cdot y_{j_2} &< 0 & (\text{jets in opposite hemispheres}) \\ |y_{j_1} - y_{j_2}| &> 4.4 & (\text{jets widely separated}) \end{aligned} \quad (7)$$

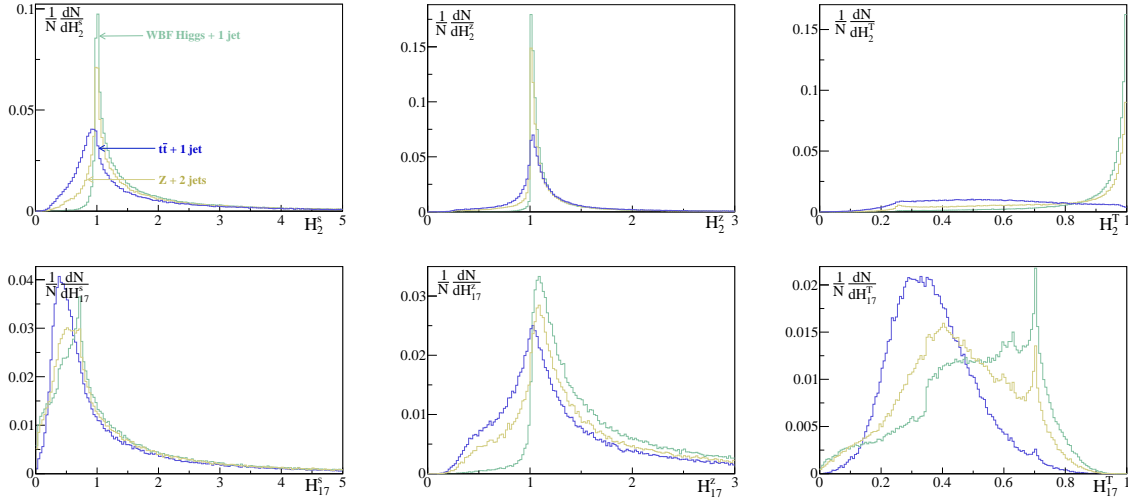


Figure 1: Fox–Wolfram moments for  $\ell = 2, 17$  with the weight factors  $W_{ij}^s$  (left),  $W_{ij}^z$  (center), and  $W_{ij}^T$  (right). All jets entering the moments pass the basic acceptance cuts of Eq.(5) and Eq.(6).

These latter two cuts have little impact after a hard invariant mass criterion of Eq.(6) and harm the extraction of the underlying coupling structure [21].

In Fig. 1 we show selected Fox–Wolfram moments for the Higgs signal and the two background processes for three of the weights shown in Eq.(4). All events pass the acceptance cuts Eq.(5) as well as the  $m_{jj}^{\min}$  condition which significantly improves the signal-to-background ratio. All jets surviving Eq.(5) and Eq.(6) are included in the moments. That is, in Fig. 1 and in Sec. IV we do not limit the moments to just two tagging jets. From the curves it is clear that  $W_{ij}^s$  is less efficient at discerning between the signal and backgrounds. This trend persists for other moments not shown. All weights except for  $W_{ij}^s$  and  $W_{ij}^z$  ensure that the range for the moments is  $0 \leq H_\ell \leq 1$  and preserve the different shapes of  $H_\ell$  for even or odd moments. Without showing detailed results we conclude that  $W_{ij}^y$  is not very efficient in extracting the WBF signal.  $W_{ij}^T$  and  $W_{ij}^p$ , and to some degree  $W_{ij}^1$ , have more power to separate the different background from the signal, so we focus on them for the rest of this paper..

For different values of  $\ell$  the Fox–Wolfram moments  $H_\ell$  reflect the strongly oscillatory behavior of the Legendre polynomials. This can be viewed as a change in the resolution with which the Fox–Wolfram moments probe the structure of the QCD jet geometry. We illustrate these patterns based on a toy model with only two final state objects,  $N = 2$ . This corresponds to the distinctive tagging jets in WBF Higgs production.

To simplify the functional form of the weights  $W_{ij}$  we denote  $|\vec{p}_2| = r_p |\vec{p}_1|$  and  $p_{T2} = r_T p_{T1}$  with  $r_{p,T} = 0 \dots 1$ . Expanding the sum in the definition Eq.(3) yields

$$H_\ell(\Omega_{12}, r) = \frac{1 + 2rP_\ell(\cos \Omega_{12}) + r^2}{1 + 2r + r^2} \quad (r = r_{p,T}) . \quad (8)$$

When the two jets are back-to-back the even and odd moments each display general properties. For all even moments  $\Omega_{12} \rightarrow \pi$  implies  $H_\ell \rightarrow 1$ , independent of  $r$ . For all odd moments, we find  $H_\ell \rightarrow 0$  in the limit  $r \rightarrow 0$ . These general trends are apparent in Fig. 2 which shows selected Fox–Wolfram moments given by Eq.(8) as a function of  $\Omega_{12}$  and  $r$ .

Also in the limit  $r \rightarrow 0$ , the Fox–Wolfram moments depend on the angle only weakly and essentially become independent of  $\ell$ . That is to say, for strongly hierarchical jets the moments defined including a momentum dependent weight are not a good descriptor of jet geometry, as all values of  $\ell$  for all values of  $\Omega_{12}$  will tend towards unity.

The power of the moments based only on two back-to-back tagging jets lies in the  $r \gtrsim 0.4$  regime. While for  $\ell = 1$  the shape of the Legendre Polynomial dominates, higher values of  $\ell$  make the Fox–Wolfram moments more sensitive to larger and larger angles between the two (tagging) jets. For moderate even  $\ell$  a pair of WBF tagging jet will typically give  $H_4 \sim 1$ , independent of  $r$ . Less widely separated jet are limited to  $H_4 \lesssim 0.5$ . Odd values, for instance  $H_5$ , have a distinct dependence on  $r$ , where WBF tagging jets will give  $H_5 \sim 1$  for

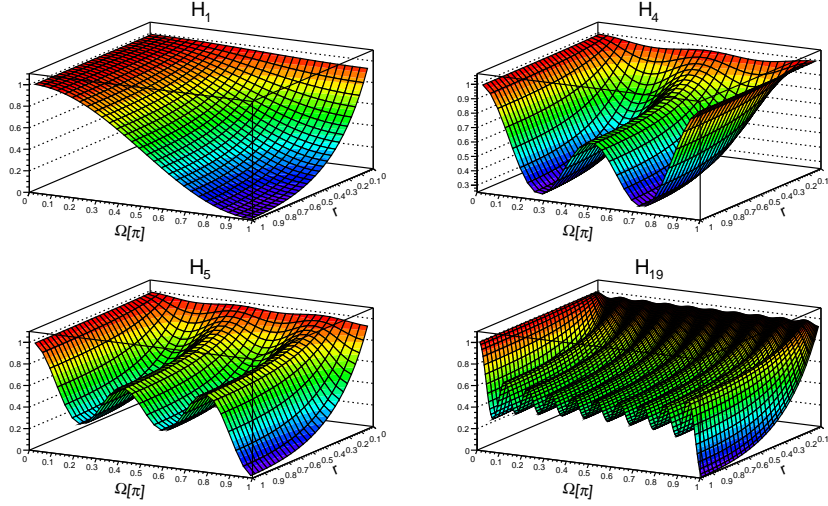


Figure 2: Fox–Wolfram moments  $H_\ell^{p,T}$  for two jets as a function of  $\Omega_{12}$  and  $r = r_{p,T}$ . We show the analytic result in our toy model. Eq.(8)

hierarchical jets with  $r \rightarrow 0$  and  $H_5 \rightarrow 0$  for balanced jets  $r \rightarrow 1$ . We will see that for typical tagging jets the maximum ranges around  $H_5 \sim 0.7$ .

Finally, large  $\ell$  values increase the sensitivity to the details of forward jet emission, for example distinguishing collinearly enhanced QCD jet radiation in  $Z$ +jets events from finite- $p_T$  tagging jets in Higgs production. As we can see in Fig. 2,  $H_{19}$  is highly sensitive to signal events peaking around  $\Omega_{12} = \pi$ . For background processes with a broad range of central jets this region has a discernibly smaller impact. Because  $H_{19}$  is an odd moment its  $r$  dependence will still lead to a strong peak around values of 0.7 for WBF events. To take away from Fig. 2, different regions in the  $(\Omega_{12}, r)$  plane translate into distinct regimes in  $H_\ell$ :

- for even  $\ell$  small values of  $H_\ell$  are not allowed; intermediate values  $0.3 \lesssim H_\ell \lesssim 0.7$  appear for democratic jet radiation  $r \gtrsim 0.4$ ; large values  $H_\ell \gtrsim 0.7$  come from three regimes: strongly ordered jets  $r \lesssim 0.4$ , collinear jets  $\Omega \lesssim 0.1$  or back-to-back jets  $\Omega \gtrsim 0.9$ .
- for odd  $\ell$  small values  $H_\ell \lesssim 0.3$  indicate symmetric back-to-back jets; intermediate values  $0.3 \lesssim H_\ell \lesssim 0.7$  correspond to relatively large  $r$  values with a sizeable angular separation; large  $H_\ell \gtrsim 0.7$  values are only possible for collinear or very hierarchical jets.

The distinction between collinear and back-to-back jets through the low- $H_\ell$  regime suggests that odd Fox–Wolfram moments are more sensitive to WBF production processes. We will test the quantitative impact of both patterns in Sec. III based on an appropriate simulation.

Once we include more than two jets, even moments can take small values. Consider for example an event with three democratic planar jets, *i.e.*  $p_{T2}/p_{T1} = 0.7$  and  $p_{T3}/p_{T1} = 0.3$ . If the hardest two jets are mostly forward-backward and the third jet is central, we obtain  $H_4^T \sim 0.2$ .

In the definition, Eq.(3), we see that the angular dependence of the Fox–Wolfram moments alone does not allow us to separate azimuthal and polar angular separation of the jets. This means that  $H^p$  will be insensitive to the details of the opening angle. However, for  $H^T$  the weight introduces a sensitivity to the polar vs azimuthal separation. This may make it possible to study the CP nature of the resonance based on the well-known differences in azimuthal angle and in rapidity between the tagging jets [21].

We can simply apply a few useful trigonometric identities and see how the Legendre polynomials  $P_\ell$  are a function of

$$\cos \Omega_{ij} = \frac{1}{2} \left[ \cos \theta_{ij}^{(+)} (1 - \cos \phi_{ij}^{(-)}) + \cos \theta_{ij}^{(-)} (1 + \cos \phi_{ij}^{(-)}) \right]. \quad (9)$$

We introduce the compact notation  $\theta_{ij}^{(+)} \equiv \theta_i + \theta_j$  and  $\theta_{ij}^{(-)} \equiv \theta_i - \theta_j$  and likewise for  $\phi_{ij}^{(\pm)}$ . Weighting  $H_\ell^T$  with  $p_T$  introduces a dependence on the polar angle through

$$p_{Ti} p_{Tj} = |\vec{p}_i| |\vec{p}_j| \sin \theta_i \sin \theta_j = \frac{|\vec{p}_i| |\vec{p}_j|}{2} \left( \cos \theta_{ij}^{(-)} - \cos \theta_{ij}^{(+)} \right), \quad (10)$$

so the full dependence of  $H_\ell$  on the angular correlations becomes

$$H_\ell^T = \frac{1}{2p_{T,tot}^2} \sum_{i,j=1}^N |\vec{p}_i| |\vec{p}_j| \left( \cos \theta_{ij}^{(-)} - \cos \theta_{ij}^{(+)} \right) P_\ell(\theta_{ij}^{(\pm)}, \phi_{ij}^{(-)}) . \quad (11)$$

### III. TWO TAGGING JETS

Tagging jets are the key to identifying Higgs bosons with a decay to tau pairs. In addition, they allow us to extract weak-boson-fusion events from the large gluon-fusion background, one of the key ingredients to a Higgs coupling measurement [22]. Usually, we require (at least) two additional jets fulfilling the conditions in Eqs.(5)-(7). In addition, the Higgs decay products have to lie centrally between the two tagging jets, a requirement we do not make explicit because we omit any information about the Higgs decay product for the sake of a most general study. Eventually, it can be added to further improve the signal-to-background ratios quoted in our analysis. From the study of Higgs coupling structures we know that Eq.(7) with an explicit cut on  $\Delta y_{jj}$  removes one of the most promising observables from the analysis [21].

In this section we use Fox–Wolfram moments *only for the leading two tagging jets* in the Higgs signal and the  $Z$ +jets and  $t\bar{t}$ +jets backgrounds, i.e. we replace Eq.(3) by

$$H_\ell^{p,T} = \sum_{i,j=1}^2 W_{ij}^{p,T} P_\ell(\cos \Omega_{ij}) . \quad (12)$$

Additional contributions from QCD jets will enter in Sec. IV. Without touching a general jet veto, we nevertheless apply a  $b$  veto to the top pair background, i.e. we veto  $b$  jets from the top decays fulfilling

$$p_{Tb} > 20 \text{ GeV} \quad |y_b| < 2.5 \quad (13)$$

with an efficiency of 60%. We show the cut flow for this very basic jet-only analysis in Tab. I. It will serve as a baseline to evaluate the performance of cutting on Fox–Wolfram moments in addition to the standard WBF cuts. All numbers in Tab. I should be taken with a grain of salt. They only include part of the information from the actual WBF  $H \rightarrow \tau\tau$  analysis [9], where we achieve a signal-to-background ratio  $S/B = \mathcal{O}(1)$ . What is important for our considerations is only the efficiency of the shown cuts in rejecting backgrounds.

Using all events passing the  $m_{jj}^{\min}$  cut in Tab. I we evaluate a set of Fox–Wolfram moments in order to estimate their power in improving the weak-boson-fusion Higgs search. The first question is if we can replace the cuts on  $y_1 \cdot y_2$  and on  $\Delta y_{jj}$  with Fox–Wolfram moments computed from the two tagging jets. In Fig. 3 we show  $H_\ell^{p,T}$  for a set of even (left two columns) and odd (right two columns) moments. In general, both of them distinguish equally well between signal and backgrounds, with a slight quantitative advantage for even  $H_\ell^T$ . Only looking at the two tagging jets the  $Z$ +jets background with its forward jet radiation tends to be similar to the signal. The  $m_{jj}^{\min}$  cut has removed most of the  $Z$ +jets events which look significantly different from the Higgs signal while the hard and central decay jets in top pair production tend to have a more unique shape. As we will see in Sec. IV the key to distinguishing WBF  $H$ +jets production from QCD  $Z$ +jets production is the jet activity in addition to the two tagging jets [12–14].

acceptance	WBF $H + 2$ jets		QCD $Z + 2$ jets		$t\bar{t} + 1$ jet		S/B
	% fail	$\sigma(\text{fb})$	% fail	$\sigma(\text{fb})$	% fail	$\sigma(\text{fb})$	
		18.7		115000		17200	1/7070
$p_{Tj} > 20 \text{ GeV}$	29.4	13.2	93.2	7820	9.63	15500	1/1767
$ y_j  < 5.0$	1.49	13.0	0.97	7740	0.182	15500	1/1788
$\Delta R_{jj} > 0.7$	2.73	12.6	3.84	7440	2.32	15100	1/1789
$m_{jj} > 600 \text{ GeV}$	68.9	3.92	96.6	253	95.8	634	1/226
$b$ -veto	0	3.92	0	253	54.0	292	1/139
$y_1 \cdot y_2 < 0$	1.41	3.86	9.17	230	13.8	252	1/125
$\Delta y_{jj} \geq 4.4$	13.9	3.32	31.8	157	66.1	85.4	1/73

Table I: Cut flow of the signal and background processes after the cuts Eq.(5)-(7) and the  $b$  veto defined in Eq.(13). The rates include the branching ratios  $H, Z \rightarrow \tau^+ \tau^-$  and two leptonic top quarks, but no requirements on the leptons. The usual cuts requiring central Higgs decay products of the central jet veto are not applied in this table.

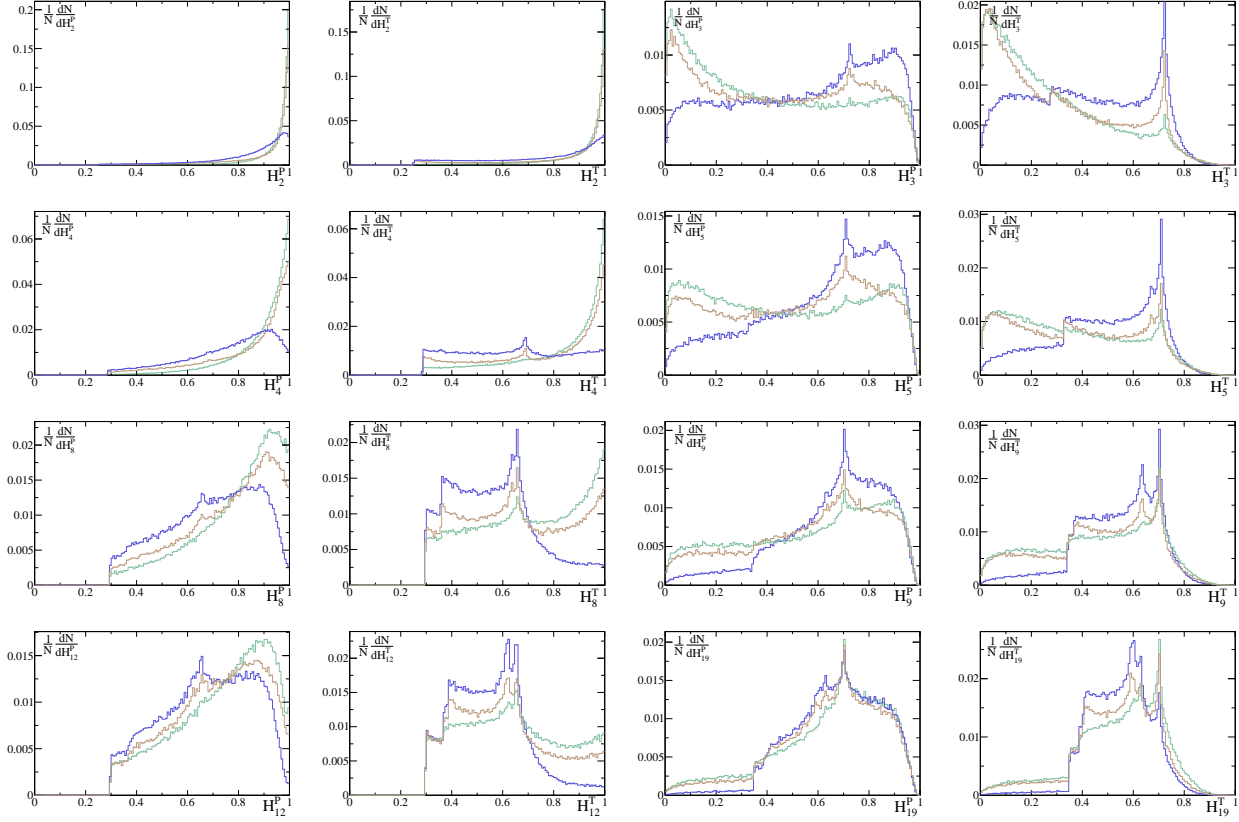


Figure 3: Normalized distributions of Fox-Wolfram moments computed only from the two tagging jets for  $\ell = 2 - 5, 8, 9, 12, 19$  with weight factors  $W_{ij}^p$  (left) and  $W_{ij}^T$  (right) for WBF H signal (green), Z+2 jets (brown) and  $t\bar{t}$ +1 jet (blue). All events pass the cuts Eq.(5) and Eq.(6).

$H_0$  and  $H_1$  do not have sufficient resolution to discriminate signal and backgrounds and are not shown. The first non-trivial even moment  $H_2$  shows a narrow peak for the Higgs signal, but even the top pair background does not look significantly different. As discussed in Sec. II even moments do not take values  $H_\ell^{p,T} \lesssim 0.3$ . The lowest odd moment,  $H_3$ , shows the events with back-to-back jets in the low- $H_3^T$  regime. The Higgs and Z topologies clearly prefer this region, with 62% and 55% of their events giving  $H_3^T < 0.3$ . Note that this percentage is nowhere close to 100%, which means that the back-to-back criterion imposed by  $H_3^T$  is harder than even the typical signal events can pass. In contrast, top pairs reside in the intermediate regime with a peak at  $H_3 \sim 0.7$ , only 35% of them lie below  $H_3^T < 0.3$ . Large values of  $H_3$  only appear for  $H_3^p$ , independent of the production mechanism. The reason is that the entire momentum instead of just its transverse direction gives a smaller ratio  $r_p$  for not quite balanced jets in the beam direction.

Moving towards larger values of  $\ell$  the odd moments become less sensitive because  $H_\ell$  resolves forward jets better. Eventually, most of the WBF Higgs are not sufficiently back-to-back to contribute to the low- $H_\ell$  regime.

	WBF $H + 2$ jets		QCD $Z + 2$ jets		$t\bar{t} + 1$ jet		S/B
acceptance	% fail	$\sigma(\text{fb})$	% fail	$\sigma(\text{fb})$	% fail	$\sigma(\text{fb})$	
$b$ -veto		3.92		253		292	1/139
$H_3^T < 0.3$	38.4	2.41	44.4	141	64.6	103	1/101
$H_4^T > 0.8$	35.8	2.52	48.1	131	73.3	78.0	1/83
$H_8^T > 0.7$	50.1	1.96	60.5	100	81.6	53.7	1/78
$H_{12}^T > 0.7$	64.5	1.39	73.0	68.3	88.0	35.0	1/74

Table II: Cut flow of the signal and background processes applying cuts on the Fox-Wolfram moments of Eq.(12) weighted with  $p_T$ , calculated with only the two leading jets. The first line starts from the event numbers after the  $m_{jj}^{\min}$  cut and the  $b$ -veto in Tab.I.

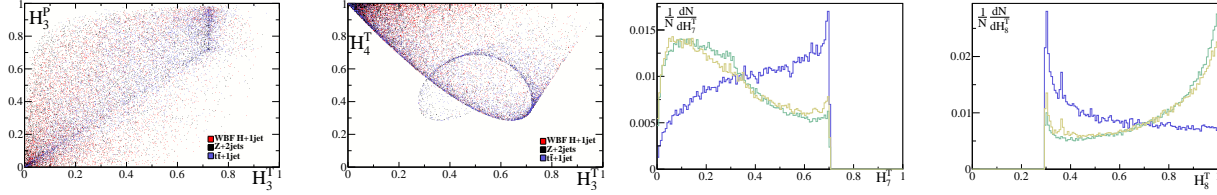


Figure 4: Left: correlations between  $H_3^T$  with  $H_3^P$  and  $H_4^T$  computed from the two tagging jets alone. Right: Normalized distributions for  $H_3^T$  and  $H_4^T$  computed from the two tagging jets alone and after requiring  $H_3^T < 0.3$ . All events in this figure pass the basic cuts Eq.(5) and Eq.(6), but not the final  $\Delta y_{jj}$  requirement.

In that situation the even moments  $H_4^T$  to  $H_8^T$  turn out more useful. Their regimes  $r \lesssim 0.4$  and  $\Omega > 0.9$  are merged and allow us to reject top pairs not only based on the geometry of the tagging jets but also on the  $p_T$  hierarchy between them. In the range  $H_4^T > 0.7$  which includes back-to-back configurations as well as strongly ordered jets, we find 76% of the Higgs events, 62% of the  $Z$ +jets background, and 40% of the top pair events. Because the resolution of  $H_3$  and  $H_4$  is similar, cutting on  $H_4^T$  does not only extract the typical WBF back-to-back tagging jet geometry. This correlation is further watered down when we replace  $H^T$  by  $H^P$ .

To answer the first question about replacing the  $\Delta y_{jj}$  cut we show results for cuts on the different Fox–Wolfram moments in Tab. II. As suggested above we start by removing the large- $H_3^T$  events. Alternatively, we can require large values for medium- $\ell$  even moments. Indeed, it is possible to separate signal and background events using Fox–Wolfram moments.  $Z$ +jets events are more similar to the Higgs signal than top pair production, just as expected. Compared to the geometric cut benchmarks shown in Tab. I the Fox–Wolfram moments based on two tagging jets achieve a similar improvement of  $S/B$  but with significantly smaller efficiencies. While they are indeed sensitive to the geometry of the jets from the hard production process, QCD jet radiation, or decays, they cannot entirely replace the well-known geometric cuts in WBF analyses [8–10].

Before moving on, we need to study correlations between the different moments, because we know from Sec. II that different kinds of events populate well-defined regions for different Fox–Wolfram moments. It is fairly obvious that even or odd moments are correlated among themselves. Following Sec. II an increase in  $\ell$  for even or odd moments dominantly increases the resolution for example in the back-to-back regime. The answer is less obvious when we consider correlations between even and odd moments or between different weights  $W^{p,T}$ . In Fig. 4 we show the correlations between the useful  $H_3^T$  and its full-momentum counterpart  $H_3^P$  as well as the closest even moment  $H_4^T$ . Both show a clear correlation, but with significant deviations from the dominant pattern. To quantify the effect of correlations on the analysis we first require  $H_3^T < 0.4$  and then show higher Fox–Wolfram moments only based on the remaining events. Surprisingly, the just slightly higher odd moment  $H_5^T$  still shows significant potential in separating signal and backgrounds. The even moment  $H_8^T$  retains essentially all its distinguishing features, no matter if we cut on  $H_3^T$  or not. This suggests that we should treat the different Fox–Wolfram moments as correlated, but by no means reducible to one even and one odd pattern.

If Fox–Wolfram moments computed from the two tagging jets alone cannot replace geometric cuts altogether, the question becomes how much they add after all the geometric cuts listed in Tab. I. In Fig. 5 we show a selected set of transverse Fox–Wolfram moments  $H^T$  for signal and background events after applying all cuts including  $\Delta y_{jj} > 4.4$  defined in Eq.(7). At this stage the usual WBF cuts on the tagging jets have been exhausted. Some of the even  $H_\ell^T$  distributions clearly distinguish top pair production on the one hand from  $H$ +jets and  $Z$ +jets on the other. Unfortunately, not even the large- $\ell$  moments will be able to clearly distinguish between Higgs and  $Z$  production. Any kind of improvement in  $S/B$  will only arise because of a reduction of the top background. As an example, following Fig. 5 we can require  $H_{12}^T > 0.7$  to improve  $S/B \sim 1/73$  to  $1/57$ , but without a beneficial effect on  $S/\sqrt{B}$ .

Summarizing the analysis of Fox–Wolfram moments computed from tagging jets only, the moments will not replace kinematic cuts on the tagging jet geometry altogether. However, they add useful information on the Higgs signal and the  $Z$ +jets and  $t\bar{t}$  backgrounds at different stages of the analysis. Even after applying all the usual WBF tagging jet cuts, the top pair background in particular can be further suppressed just based on the tagging jet correlations phrased in terms of  $H_\ell$ . Moreover, the different moments are less correlated than one might have guessed from the toy model discussed in Sec. II.



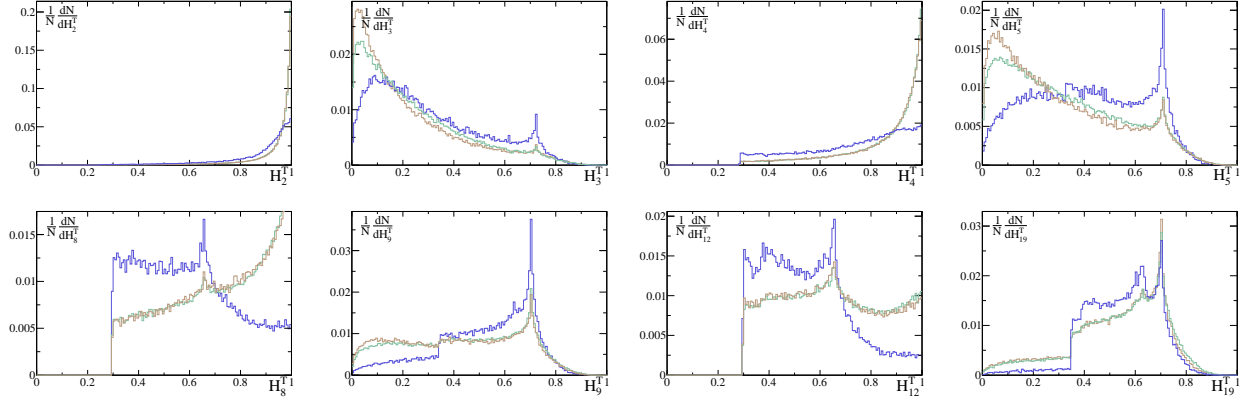


Figure 5: Normalized distributions of Fox-Wolfram moments computed from the two tagging jets only for  $\ell = 2 - 5, 8, 9, 12, 19$  with a weight factors  $W_{ij}^T$  for WBF H+1 jet signal (green), Z+2 jets (brown) and  $t\bar{t}$ +1 jet (blue). All events pass the full set of QCD cuts Eqs.(5)-(7).

#### IV. ALL JETS

In addition to the hallmark tagging jets with a very large invariant mass and sizeable transverse momentum the key to WBF Higgs analysis is the reduced central jet activity. It can be understood in two different ways.

First, weak boson fusion does not include any color correlations between the two quark legs. In that sense, it consists of two distinct deep inelastic scattering processes. QCD corrections involving a gluon exchange between

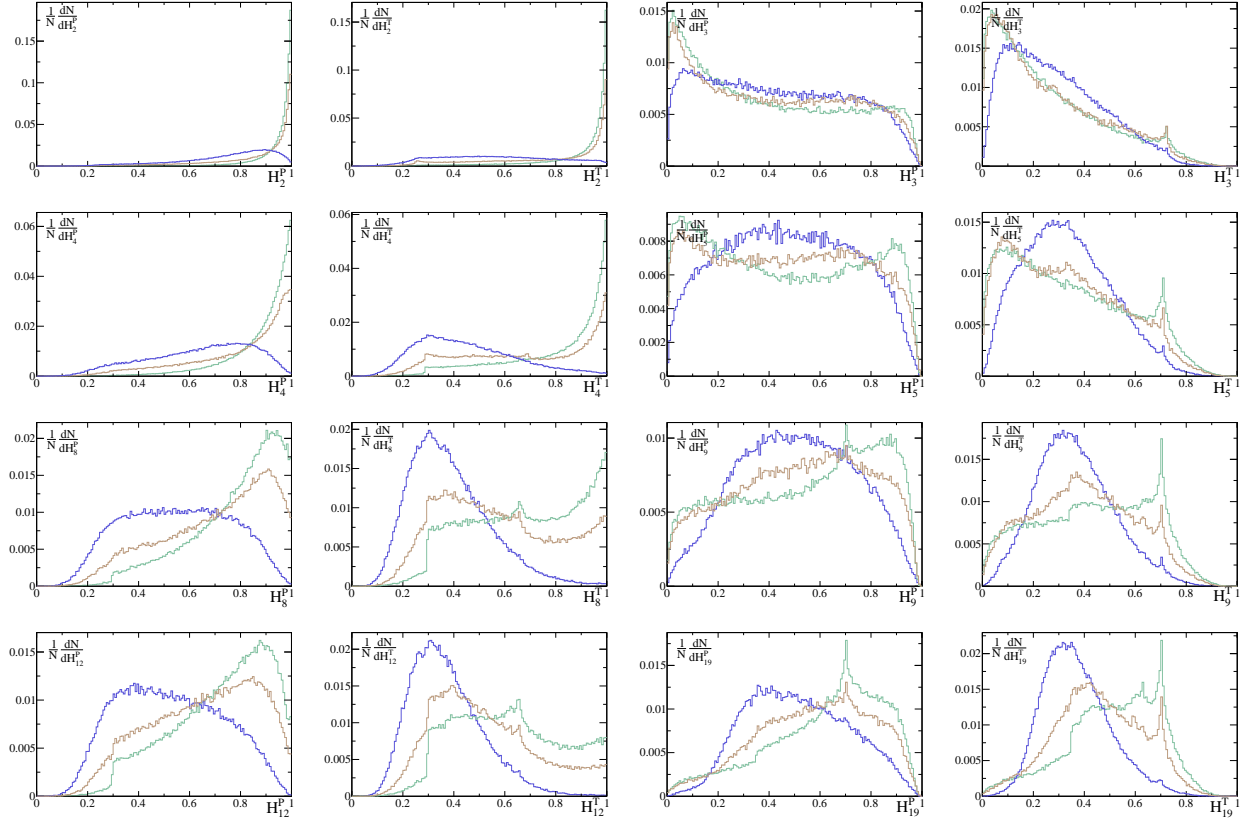


Figure 6: Normalized distributions on Fox-Wolfram moments computed from all available jets for  $\ell = 2 - 5, 8, 9, 12, 19$  with weight factors  $W_{ij}^P$  (left) and  $W_{ij}^T$  (right) for WBF H+1 jet signal (green), Z+2 jets (brown) and  $t\bar{t}$ +1 jet (blue). All events pass the cuts Eq.(5) and Eq.(6).

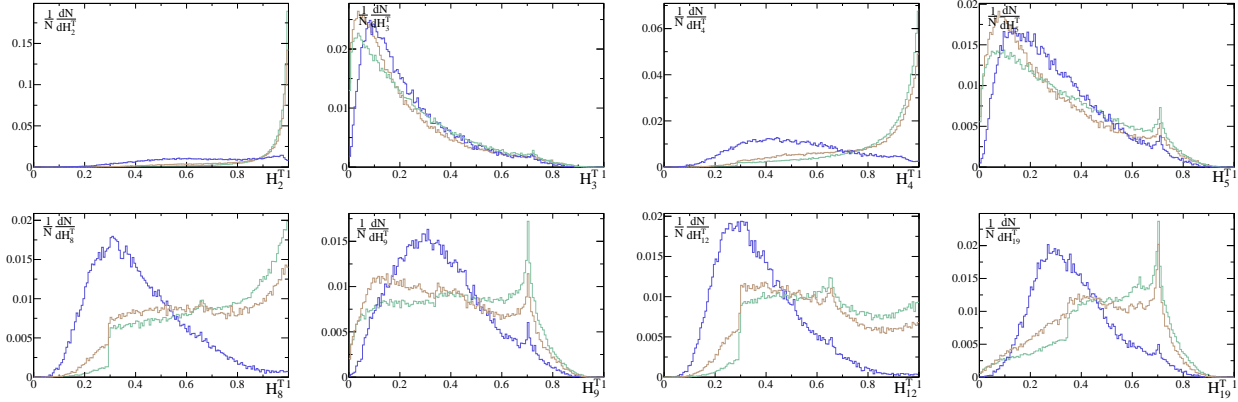


Figure 7: Normalized distributions of Fox–Wolfram moments computed from all jets for  $\ell = 2 - 5, 8, 9, 12, 19$  with a weight factor  $W_{ij}^T$  for WBF H+1 jet signal (green), Z+2 jets (brown) and  $t\bar{t}$ +1 jet (blue). All events pass the full set of QCD cuts, Eqs.(5)-(7).

the two quark legs are exactly zero. The only source of small virtual gluon contributions is the interference between the two diagrams with exchanged tagging jets, but with hardly any common phase space. Just like virtual gluon exchange central, real gluon emission between the two tagging jets is strongly suppressed. QCD radiation only occurs in the direction of the incoming and outgoing quark legs [12].

Alternatively, we can study the jet radiation pattern by counting additional jets. For any kind of background process the large value of  $m_{jj}$  generates an enhanced probability for central jet radiation, leading to a Poisson distribution in the number of jets. For the WBF signal the large values of  $m_{jj}$  are natural, so the radiation pattern remains staircase, with a significantly reduced radiation probability for the first few emissions [13].

Independent of the physics picture, the reduced radiation of central jets is usually exploited by a central jet veto above a  $p_T$  threshold around 20 GeV. The question is if we can make use of the geometry of these additional jets instead of or before throwing them away [23].

Just like in Sec. III we show a set of Fox–Wolfram moments for the Higgs signal and the two backgrounds. The only difference between Fig. 6 and Fig. 3 is that instead of only the tagging jets we now include all jets passing Eq.(5) in the definition of the moments, Eq.(3). All events pass the  $m_{jj}^{\min}$  cut in Tab. I. Again, we show the two different weights  $H_\ell^p$  and  $H_\ell^T$ . The Fox–Wolfram moments based on all jets are not very different from those based on the tagging jets only, except that for even moments the additional jets can in principle populate  $H_\ell^T < 0.3$  due to the central jet activity as discussed in the toy example for three planar jets at the end of Sec. II. Specifically for the Higgs signal, the majority of events do not even have an additional hard jet, so the two distributions are largely identical. Even moments are still largely limited to  $H_\ell^T > 0.3$  and show a clear peak towards  $H_\ell^T \sim 1$ . However, for Z+jets some moments change, starting with  $H_4^T$  and giving very visible differences between the Higgs signal and the Z background for  $H_8^T$  or  $H_{10}^T$ . This is not entirely unexpected, because a veto on additional jets can also distinguish these two channels. Top pair production with three relatively hard jets, two from the top decays and one from QCD radiation, shows a distinct peak for example around  $H_8^T \sim 0.3$ .

From Sec. III we know that Fox–Wolfram moments are not sufficiently effective to replace the tricky  $\Delta y_{jj}$  cut in the standard WBF analyses. In Fig. 7 we show the same moments with the transverse weight factor including all WBF cuts Eqs.(5)-(7). As expected, the sensitivity to the differences in H+jets and Z+jets production is reduced. Jets radiated off the hard WBF process and QCD jet radiation become very similar at this stage. The most noticeable difference is that the Z+jets background tends towards smaller even moments without the sharp edge around  $H_\ell^T = 0.3$ . This effect is numerically limited because the usual weights  $W_{ij}$  in the Fox–Wolfram moments penalize jets with low (transverse) momentum, so soft additional jets have relatively little impact. This is different for the hard top decay jets, so we see that high even moments  $H_8^T$  or  $H_{12}^T$  can be used to remove events where the addition non-tagging jets have a visible impact. A simple cut on one of these moments can improve  $S/B$  from the value 1/73 quoted in Tab. I to 1/50, keeping the majority of signal events.

To understand further how the low (transverse) momentum jets are restricted by the presence of momentum dependent weights, we show moments with unit weight  $W_{ij}^1$  in Fig. 8. The most noticeable difference in comparison to Fig. 7 are the sharper peaks in the H+jets and Z+jets distributions due to the uninhibited

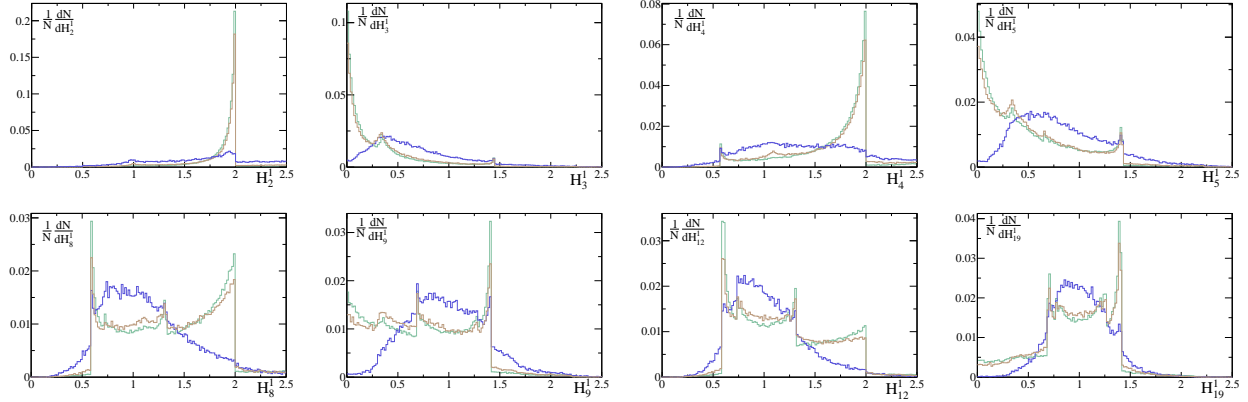


Figure 8: Normalized distributions of Fox–Wolfram moments computed from all jets for  $\ell = 2-5, 8, 9, 12, 19$  with weight factor  $W_{ij}^1$  for WBF  $H+1$  jet signal (green),  $Z+2$  jets (brown) and  $t\bar{t}+1$  jet (blue). All events pass the full set of QCD cuts, Eqs.(5)-(7).

presence of softer jet radiation. This can be better understood in the  $H$ +jets and  $Z$ +jets case, where there are typically only two jets passing the full set of QCD cuts of Eq.(5)-(7), by referring to the two-jet toy model of Sec. II in the case  $r = 1$ . Here we see for example that the sharp peaks at low  $H_\ell^1$  correspond to small total angles between the jets which are not dampened with a choice of unit weight.

It is also worth emphasizing that because the moments are not defined with respect to a preferred axis, they cannot select jets in a specific region. Hence, the moments cannot be used to, for instance, emphasize central jets in the absence of forward-backward jet activity. We verified this using  $W_{ij}^y$  of Eq.(4) as a weight that favors low rapidity jets. While  $H_\ell^T$  cannot replace a jet veto altogether, it certainly includes useful information which will improve the WBF analysis. As shown in Fig. 4, Fox–Wolfram moments should be included as a somewhat correlated set of new observables.

## V. OUTLOOK

In this first study we have shown that Fox–Wolfram moments [1] based on jets are very useful tools to improve many LHC analyses benefiting from information about the QCD structure of signal and background events. Our example process is weak-boson-fusion Higgs production with tagging jets described by the hard matrix element. Two leading backgrounds are  $Z$ +jets where the tagging jets come from QCD radiation and top pair production, where at least one of the tagging jets will be a top decay jet.

For weak boson fusion the key questions are how much information we can extract from the Fox–Wolfram moments before we apply a cut on the rapidity separation of the two tagging jets or before we apply a jet veto. We have shown that moments either based on the two tagging jets alone or based on all jets in the event show distinctly different features for the three signal and background processes. We have tested different weights entering the definition of the Fox–Wolfram moments in Eq. (3). At least for the tagging jets a weight based on transverse momenta is the most useful [2]. On the other hand, for a study of the jet activity, alternative weights might be helpful. In addition, we have seen that the full set of odd and even moments cannot be reduced to one or two representative moments; they should be considered as a new class of correlated but individually useful LHC observables.

Clearly, we did not present a conclusive final study on Fox–Wolfram moments at the LHC. Many aspects can and have to be improved, from the physical objects entering the moments to the choice of weights or an exhaustive study of their correlations. In an era where we are becoming more and more confident in exploiting QCD features for many LHC analyses Fox–Wolfram moments have the potential to play a key role as universal analysis tools.

### Acknowledgments

We would like to thank Peter Schichtel for his technical help at many different stages of this project.

- 
- [1] G. C. Fox and S. Wolfram, Phys. Rev. Lett. **41**, 1581 (1978).
  - [2] R. D. Field, Y. Kanev and M. Tayebnejad, Phys. Rev. D **55**, 5685 (1997).
  - [3] P. W. Higgs, Phys. Lett. **12**, 132 (1964); P. W. Higgs, Phys. Rev. Lett. **13**, 508 (1964); F. Englert and R. Brout, Phys. Rev. Lett. **13**, 321 (1964).
  - [4] for LHC reviews e.g. A. Djouadi, Phys. Rept. **457**, 1 (2008); T. Plehn, Lect. Notes Phys. **844**, 1 (2012) [arXiv:0910.4182 [hep-ph]].
  - [5] D. E. Morrissey, T. Plehn and T. M. P. Tait, Phys. Rept. **515**, 1 (2012); H. Dreiner, M. Krämer and J. Tattersall, arXiv:1211.4981 [hep-ph].
  - [6] G. Aad *et al.* [ATLAS Collaboration], Phys. Lett. B **716**, 1 (2012).
  - [7] S. Chatrchyan *et al.* [CMS Collaboration], Phys. Lett. B **716**, 30 (2012).
  - [8] N. Kauer, T. Plehn, D. Rainwater and D. Zeppenfeld, Phys. Lett. B **503**, 113 (2001).
  - [9] D. L. Rainwater, D. Zeppenfeld and K. Hagiwara, Phys. Rev. D **59**, 014037 (1999); T. Plehn, D. L. Rainwater and D. Zeppenfeld, Phys. Rev. D **61**, 093005 (2000).
  - [10] D. L. Rainwater and D. Zeppenfeld, JHEP **9712**, 005 (1997); J. R. Andersen, C. Englert and M. Spannowsky, arXiv:1211.3011 [hep-ph].
  - [11] R. Kleiss and W. J. Stirling, Phys. Lett. B **200**, 193 (1988); U. Baur and E. W. N. Glover, Phys. Lett. B **252**, 683 (1990); V. D. Barger, K. Cheung, T. Han, J. Ohnemus and D. Zeppenfeld, Phys. Rev. D **44**, 1426 (1991).
  - [12] D. L. Rainwater, R. Szalapski and D. Zeppenfeld, Phys. Rev. D **54**, 6680 (1996).
  - [13] E. Gerwick, T. Plehn and S. Schumann, Phys. Rev. Lett. **108**, 032003 (2012).
  - [14] B. E. Cox, J. R. Forshaw and A. D. Pilkington, Phys. Lett. B **696**, 87 (2011).
  - [15] for a nice overview of LHC applications see e.g. A. Banfi, G. P. Salam and G. Zanderighi, JHEP **1006**, 038 (2010).
  - [16] T. Sjostrand, L. Lonnblad, S. Mrenna and P. Z. Skands, hep-ph/0308153.
  - [17] S. Asai, G. Azuelos, C. Buttar, V. Cavasinni, D. Costanzo, K. Cranmer, R. Harper and K. Jakobs *et al.*, Eur. Phys. J. C **32S2**, 19 (2004).
  - [18] T. Gleisberg, S. Höche, F. Krauss, M. Schönherr, S. Schumann, F. Siegert and J. Winter, JHEP **0902**, 007 (2009).
  - [19] S. Catani, F. Krauss, R. Kuhn and B. R. Webber, JHEP **0111**, 063 (2001).
  - [20] M. Cacciari, G. P. Salam and G. Soyez, Eur. Phys. J. C **72**, 1896 (2012).
  - [21] T. Plehn, D. L. Rainwater and D. Zeppenfeld, Phys. Rev. Lett. **88**, 051801 (2002); C. Ruwiedel, N. Wermes and M. Schumacher, Eur. Phys. J. C **51**, 385 (2007); C. Englert, D. Goncalves-Netto, K. Mawatari and T. Plehn, arXiv:1212.0843 [hep-ph].
  - [22] see e.g. M. Klute, R. Lafaye, T. Plehn, M. Rauch and D. Zerwas, Phys. Rev. Lett. **109**, 101801 (2012).
  - [23] for a similar idea see e.g. C. Englert, M. Spannowsky and M. Takeuchi, JHEP **1206**, 108 (2012).